M. Gabriela Espinosa
Saint Louis University,
3507 Lindell Boulevard,
Saint Louis, MO 63103
e-mail: mgespinosa@wustl.edu

William S. Gardner
Saint Louis University,
3507 Lindell Boulevard,
Saint Louis, MO 63103
e-mail: wgardner@slu.edu

Lisa Bennett
Saint Louis University,
3507 Lindell Boulevard,
Saint Louis, MO 63103
e-mail: ljbenn.lb@gmail.com

Bradley A. Sather
Saint Louis University,
3507 Lindell Boulevard,
Saint Louis, MO 63103
e-mail: sather_brad@yahoo.com

Hiromi Yanagisawa
University of Texas Southwestern,
6000 Harry Hines Boulevard NA5.320,
Dallas, TX 75390-9148
e-mail: hiromi.yanagisawa@utsouthwestern.edu

Jessica E. Wagenseil
Washington University,
1 Brookings Drive, CB 1185,
Saint Louis, MO 63130
e-mail: jessica.wagenseil@wustl.edu

The Effects of Elastic Fiber Protein Insufficiency and Treatment on the Modulus of Arterial Smooth Muscle Cells

Elastic fibers are critical for the mechanical function of the large arteries. Mechanical effects of elastic fiber protein deficiency have been investigated in whole arteries, but not in isolated smooth muscle cells (SMCs). The elastic moduli of SMCs from elastin (Eln-/-) and fibulin-4 (Fbln4-/-) knockout mice were measured using atomic force microscopy. Compared to control SMCs, the modulus of Eln-/- SMCs is reduced by 40%, but is unchanged in Fbln4-/- SMCs. The Eln-/- SMC modulus is rescued by soluble or α elastin treatment. Altered gene expression, specifically of calponin, suggests that SMC phenotypic modulation may be responsible for the modulus changes. [DOI: 10.1115/1.4026203]

Introduction

Increased arterial stiffness is directly correlated with hypertension and cardiovascular disease [1]. Passive stiffness of the conducting arteries is largely determined by the extracellular matrix (ECM) proteins in the wall, such as collagen and elastic fibers, produced by the smooth muscle cells (SMCs) found in the medial layer. The medial layer is organized into concentric lamellar units, made up of elastic fibers, with circumferentially arranged SMCs and bundles of collagen fibers [2–4]. During elastic fiber assembly, the SMCs secrete soluble tropoelastin that is organized with the assistance of additional proteins, such as members of the fibulin and fibrillin families, for crosslinking into insoluble elastin by lysyl oxidase [5].

The roles of various elastic fiber proteins in arterial mechanics and cardiovascular function have been investigated using genetically modified mice. Newborn mice lacking the elastin protein (*Eln*-/-) have increased arterial wall stiffness, SMCs with altered proliferation, migration and morphology, and die shortly after birth [1,6]. Elastin haploinsufficient mice (*Eln*+/−) produce only half of the elastin amounts found in unaffected mice (*Eln*+/+). *Eln*+/− mice have a full life span, despite the higher number of lamellar units, increased arterial stiffness, and resulting hypertension [7,8]. Humans with elastin haploinsufficiency have supravalvular aortic stenosis, characterized by narrowing of the ascending aorta and hypertension [9]. Newborn mice lacking the fibulin-4 protein (*Fbln4*-/-) also die shortly after birth with severe lung and vascular defects. Elastic tissues from *Fbln4*-/- mice, such as lung, skin, and arteries, show no decrease in elastin content, but have reduced elasticity due to disrupted elastic fibers [10]. Mice with a SMC-specific knockout of *Fbln4* (SMKO), have ascending aortic aneurysms [11]. Humans with fibulin-4 mutations have been diagnosed with aneurysms, emphysema, and cutis laxa [12].

The mechanical properties of arteries from *Eln*-/- [13], *Eln*+/− [7], and SMKO mice [14] have been previously reported, but there has been little focus on the mechanical properties of isolated SMCs from mice deficient in elastic fiber proteins. Atomic force microscopy (AFM) has been used to directly measure the elastic modulus of isolated SMCs exposed to different conditions, inhibitors, or treatments [15,16]. Recent experiments comparing arterial SMCs from old and young animals suggest that mechanical properties of the SMCs themselves may contribute to changes in arterial wall stiffness [17]. These same experiments used fluorescent f-actin labeling to show a correlation between increased cell stiffness and a higher density of actin stress fibers. Hence, we measured the modulus of isolated arterial SMCs from elastin and fibulin-4 deficient mice using AFM. In addition, we studied the effects of two elastin treatments on the modulus of SMCs from *Eln*+/+ and *Eln*-/- mice. Differences between the treatments may elucidate the importance of soluble versus crosslinked elastin in modulating SMC mechanical properties. Actin stress fiber density in treated and untreated cells was examined and compared between groups, anticipating increased actin amounts with increased stiffness. We also measured changes in SMC gene expression using quantitative RT-PCR. This work may identify a genetic mechanism for the changes in SMC modulus and will

Contributed by the Bioengineering Division of ASME for publication in the Journal of Biomechanical Engineering. Manuscript received August 29, 2013; final manuscript received December 2, 2013; accepted manuscript posted December 11, 2013; published online February 5, 2014. Editor: Victor H. Barocas.

Table 1 Force spectroscopy experimental design

Study	No. of trials	Genotypes	Minimum No. of SMCs/Genotype
Location	1	*Eln*-/-, *Eln*+/−, and *Eln*+/+	21
Elastin Deficiency	3	*Eln*-/-, *Eln*+/−, and *Eln*+/+	13
Fibulin-4 Deficiency	3	*Fbln4*-/-, *Fbln4*+/−, and *Fbln4*+/+	20
Soluble Elastin Treatment	4	*Eln*-/- and *Eln*+/+	20
Alpha Elastin Treatment	3	*Eln*-/- and *Eln*+/+	20

contribute to the understanding of how SMC gene expression and mechanical properties impact overall arterial mechanics.

Materials and Methods

SMC Isolation. All animal studies were performed according to protocols approved by the Institutional Animal Care and Use Committee. *Eln*+/− C57BL/6J [8] mice were mated to produce litters consisting of *Eln*+/+, *Eln*+/−, and *Eln*-/- pups. *Fbln4*+/− C57BL/6J [11] mice, generated by backcrossing *Fbln4*+/− 129/C57BL/6J to C57BL/6J for nine generations, were mated to produce litters consisting of *Fbln4*+/+, *Fbln4*+/−, and *Fbln4*-/- pups. One-day old pups were euthanized via CO_2 asphyxiation. Tail samples were used to determine each pup's genotype. While maintaining sterility, the aorta and carotid arteries were extracted, rinsed in 10× and 1× penicillin-streptomycin (Sigma, St. Louis, MO) solutions, and digested in a 19.86 units/ml of collagenase (Worthington, Lakewood, NJ) and 0.44 units/ml of elastase (Worthington, Lakewood, NJ) solution for 90 min on a Multi-Therm shaker table set to 37 °C. All solutions were prepared in serum-free DMEM/F-12 Hams media (Sigma, St. Louis, MO). The SMCs were isolated using 400 × g centrifugation for 5 min and were resuspended in 1 ml of warmed media with 20% fetal bovine serum (FBS) (Biowest, Nuaillé, France). SMCs from the aorta and carotid arteries were harvested together in order to have a sufficient number of cells to start a viable culture. SMCs of the same genotype were cultured together until passage (P) 3, at which point they were cryopreserved in vials of 20% FBS media containing 5% dimethyl sulfoxide (DMSO).

Cell Culture. SMCs of the genotype of interest were plated on tissue culture treated T-75 flasks (Corning, Tewksbury, MA). After one week, confluent SMCs were trypsinized and plated on 60 mm tissue culture treated petri dishes, if used for AFM, or on coverslips inside a 24-well plate, if used for fluorescence microscopy. The SMCs remained in the flasks if they were used for quantitative RT-PCR. The culture vessels contained 20% FBS control media, which was replaced with either soluble elastin or fragments of crosslinked elastin (α elastin) (Elastin Products Company, MO) supplemented 20% FBS media if the treatment conditions were being studied. Both treatments were prepared at 0.16 mg/ml concentration. After one day, the SMCs were used for their respective experiments. The concentration and timeline for elastin treatment were based on previously published results showing effects of soluble elastin treatment on proliferation, adhesion, migration, and amount of actin stress fibers [18,19]. All SMCs were used between P 4 – 6.

Atomic Force Microscopy. Borosilicate 5 μm diameter beads (SPI, West Chester, PA) were attached to the C cantilever of an MLCT probe (Bruker Corporation, Camarillo, CA) using a two part marine epoxy (Progressive Epoxy Polymers, Pittsfield, NH) [20]. The PCM-90 spring constant calibrator (Novascan Technologies, Ames, IA) was used to measure the cantilever spring constant (k) in triplicate, according to the Sader method [21]. The average spring constant for cantilevers used in these experiments was 0.012 N/m. Immediately prior to AFM force spectroscopy, the media in the petri dish was replaced with 1 ml of serum and phenol red free media (Sigma, St. Louis, MO). A few drops of the same media were applied onto the probe, which was then lowered onto the petri dish of SMCs at the ambient room temperature. The parameters for the force curves were set to an indentation rate of 1000 nm/s and a maximum cantilever deflection of 1 V. The average indentation depth used was 180 nm or about 8% of the maximum height of an SMC, assuming a height of 2.3 μm [20]. Force curves were initially acquired at three locations along the length of the spindle shaped SMCs: adjacent to the nucleus, halfway between the nucleus and cell edge, and at the edge. All of the force curves for experiments following the preliminary location study were obtained at the middle site. During each experiment, or "trial," force curves were obtained from 20 SMCs or until the dish had been in the AFM for 30 min, whichever came first. Dishes of SMCs were not left in the AFM longer than 30 min because of media evaporation concerns. Table 1 summarizes the force curve protocol and number of trials for each of the studies.

Data Analysis

Manual Method. The analysis of every force curve requires the measurement and calculation of the cantilever's spring constant and the optical lever sensitivity (OLS). The former is explained above. The OLS can be measured from a force curve obtained on an undeformable surface, such as the petri dish, and in the same environment as the actual measurements, such as the cell culture media used here. Once the curve is obtained, the reciprocal of the contact region's slope is calculated and used as the OLS. Using the Novascan ESPM 3D software, all of the curves' raw data were batch processed using the appropriate k and OLS values to create force versus deformation curves.

Each force curve file was individually opened and analyzed in the software's Young's modulus window. A user-defined contact point and range, usually the entire contact region, were selected. The Hertz model was chosen for the analysis given the tip's spherical shape. The Hertz model's expression,

$$E = \frac{3}{4}\left(1-\nu^2\right)\frac{F}{\sqrt{RD^3}} \tag{1}$$

was used to calculate the modulus, E, by using measured values of force and deformation, F and D, respectively. The tip's radius, $R = 2500$ nm, was also entered. Finally, since the SMCs are assumed to be incompressible, a Poisson's ratio $\nu = 0.5$ was used. The software's results included a calculated value for Young's modulus and a fitted curve that should match the measured curve.

Automated Method. The Novascan software heavily depends on a user-defined contact point that is not always easily discerned or reproduced. A MATLAB program was developed to consistently calculate the contact point based on a previously established two part polynomial iterative approach [22],

$$h(z) = \begin{Bmatrix} a_1 + b_1 z & \text{for} \quad z \le z^{\text{trial}} \\ a_2 + b_2\left(z - z^{\text{trial}}\right) + c_2\left(z - z^{\text{trial}}\right)^2 & \text{for} \quad z > z^{\text{trial}} \end{Bmatrix} \tag{2}$$

where

$$a_2 = a_1 + b_1 z^{\text{trial}} \tag{3}$$

Table 2 Life Technologies assay ID numbers and sequence information for the Taqman gene expression assays used for RT-PCR

Gene	Protein	Assay ID No.	NCBI Reference sequence	Exon boundary	Assay location	Amplicon length
Aebp1	Adipocyte Enhancer Binding Protein 1	Mm00477402_m1	NM_009636.2	1 – 2	532	103
Acta2	SM α-Actin	Mm00725412_s1	NM_007392.2	9 – 9	1366	95
B2M	β-2 Microglobulin	Mm00437762_m1	NM_009735.3	1 – 2	111	77
Cald1	Caldesmon	Mm00513996_m1	NM_145575.3	2 – 3	403	60
Cdh2	N-Cadherin	Mm01162497_m1	NM_007664.4	9 – 10	1996	82
Col1a1	Collagen 1	Mm00801666_g1	NM_007742.3	49 – 50	4071	89
Cnn1	Calponin	Mm00487032_m1	NM_009922.4	1 – 2	167	59
Eln	Elastin	Mm00514670_m1	NM_007925.3	4 – 5	230	59
Efemp2 (Fbln4)	Fibulin-4	Mm00445429_m1	NM_001164352.1	6 – 7	1059	94
Myocd	Myocardin	Mm00455051_m1	NM_145136.4	9 – 10	1442	103
Myh10	Embryonic SM Myosin Heavy Chain	Mm00805131_m1	NM_175260.2	39 – 40	5915	61
Myh11	SM Myosin Heavy Chain	Mm00443013_m1	NM_001161775.1	15 – 16	2017	92
Smtn	Smoothelin	Mm00449973_m1	NM_001159284.1	3 – 4	350	66
Tagln	SM22	Mm00441661_g1	NM_011526.5	2 – 3	422	64

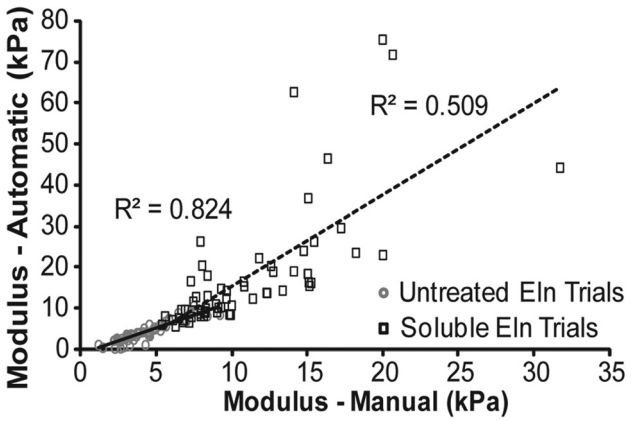

Fig. 1 Comparison of data analysis methods: low modulus values are highly correlated between the manual and automated methods, but diverge as the modulus increases

The first part of the polynomial is a linear fit to the precontact region. The second part of the polynomial is a parabolic fit to the post contact region. The intersection of these two parts is a trial contact point, z^{trial}, while the deformation at any given applied force is z. In these equations, a_1, b_1, a_2, b_2 and c_2 are constants initially guessed based on linear and polynomial fits of the pre- and postcontact regions. A series of fits are attempted and the corresponding z^{trial} x-coordinates are plotted against the fitting error. The z^{trial} value with the least fitting error is chosen as the force curve's contact point. The Hertz model is then applied from the calculated contact point to the end of the curve to calculate E.

Fluorescence Microscopy. Qualitative assessment of actin stress fiber density and organization in untreated and α elastin treated *Eln*-/- and *Eln*+/+ SMCs was performed using a monoclonal anti-actin, α-smooth muscle primary antibody produced in a mouse (A5228, Sigma, St. Louis, MO). A secondary antibody, 488 anti-mouse made in goat (T5393, Sigma, St. Louis, MO), and nuclear stain, Hoechst 33,258 (Sigma, St. Louis, MO) were also used. SMCs were grown on four coverslips for each of the four genotype-treatment combinations and arranged in a 24-well plate. The SMCs were fixed in a 4% paraformaldehyde (PFA) solution. The coverslips were transferred to an empty 24-well plate and stained following the manufacturer's protocol. Upon completion, the coverslips were mounted on glass slides. Fluorescent micrographs of each coverslip were obtained using the DAPI filter to observe the nuclear stain and the FITC filter to observe the smooth muscle α-actin stress fiber stain. Images captured at the same location were superimposed using ImageJ.

Quantitative RT-PCR. Total RNA samples from *Eln*-/- and *Eln*+/+ SMCs under all treatment conditions were isolated and used to quantitatively measure expression of an array of genes governing the production of ECM, SMC marker, and cytoskeletal proteins. The SMCs were trypsinized and neutralized with 20% FBS media. The cell solution was centrifuged at 1000 rpm for 5 min and the resulting supernatant was discarded. RNA from the cell pellet was isolated and purified using the RNeasy Mini Kit (Qiagen, Germantown, MD) following the manufacturer's instructions. The genomic DNA digestion step was performed using the RNase-Free DNase Set (Qiagen, Germantown, MD). RNA concentration and purity for each sample was measured using a NanoDrop 2000 c Spectrophotometer (Thermo Scientific). RNA samples were either stored at −80 °C or immediately used for reverse transcription. Reverse transcription was performed using the High Capacity cDNA Reverse Transcription Kit (Life Technologies, Carlsbad, CA) following the manufacturer's instructions. cDNA concentration and purity were measured using the NanoDrop spectrophotometer. The cDNA was either stored at 4 °C or amplified in the Flex 12 K RT-PCR system using Taqman gene expression assays (Cat #4331182) (Life Technologies, Carlsbad, CA). The genes examined include *Aebp1*, *Acta2*, *Cald1*, *Cdh2*, *Col1a1*, *Cnn1*, *Eln*, *Fbln4*, *Myocd*, *Myh10*, *Myh11*, *Smtn*, and *Tagln*. Beta-2 microglobulin (B2M) was used as a housekeeping gene. The assay IDs and sequence information for each gene are listed in Table 2.

Statistical Analysis. All bar graphs show the mean and standard deviation. The moduli across genotypes, for the elastin and fibulin-4 experiments, and across treatments, for the soluble and α elastin experiments, were compared using a one-way ANOVA and Bonferroni post hoc test. A one-way ANOVA with the Bonferroni post hoc test was used to compare gene expression compared to untreated *Eln*+/+ SMCs. In all cases, significance was defined as $p < 0.05$.

Results

Analysis Methods Correlate Well at Low Stiffness. Both manual and automated methods were used to calculate the modulus for the untreated and soluble elastin treated elastin deficient SMCs. The manual and automated analysis methods have a strong correlation ($R^2 = 0.824$) when the calculated modulus values are relatively low ($E < 10$ kPa). Figure 1 shows that the methods' calculations diverge and their correlation weakens ($R^2 = 0.509$) as the modulus increases ($E > 10$ kPa). Several of the high modulus cases were examined and it was noted that the calculated contact point in the automated method had a high fitting error and was unrealistic. Although the automated method is an excellent way to reduce bias and expedite analysis, it is only reliable for low modulus values as currently implemented. Therefore, the Young's modulus for all the AFM data presented in this study was calculated using the manual method.

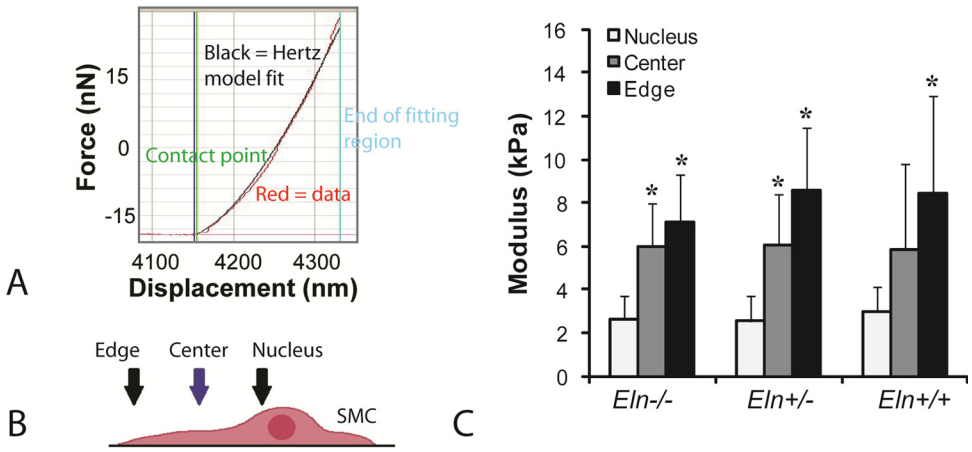

Fig. 2 Representative force-displacement curve and fitted Hertz model with the manual contact point method (*A*). Across the SMC surface (*B*) the modulus varies significantly, increasing as the AFM probe approaches the SMC edge (*C*). * = $P < 0.05$ compared to the location adjacent to the nucleus.

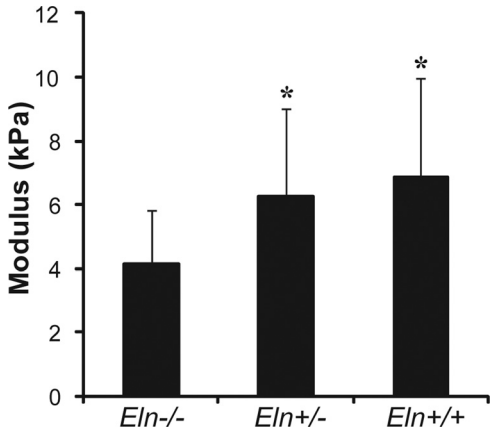

Fig. 3 Elastin deficiency significantly reduces the modulus of *Eln-/-* SMCs. * = $P < 0.05$ compared to *Eln-/-* SMCs

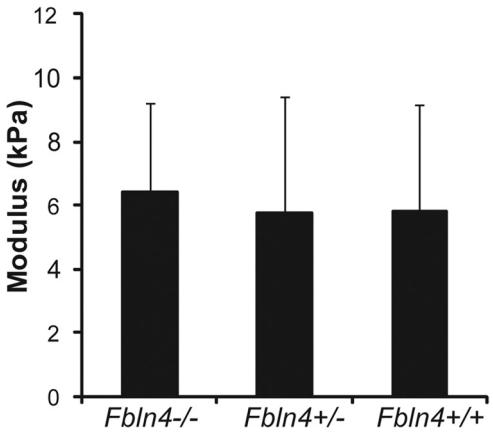

Fig. 4 Fibulin-4 deficiency has no effect on the SMC modulus

SMC Modulus Varies With Location. Figure 2(*A*) shows an example force-displacement curve with the manual contact point chosen and the fitted Hertz model overlaying the raw data. The locations along the SMC long axis for modulus measurements are shown in Fig. 2(*B*). There is an increased Young's modulus towards the edge of the cell (Fig. 2(*C*)). For all genotypes, the Young's modulus values at the edge are significantly greater than those measured adjacent to the nucleus, with up to a 236% change. Similarly, the center location's modulus shows up to a 137% increase compared to the nuclear site. While no differences in the modulus at each location were found between genotypes in this preliminary experiment, only one trial of the location experiment was performed during training of the AFM operator to determine the optimal indentation location for additional experiments. The center location was chosen for additional experiments by the trained AFM operator to avoid variations near the cell nucleus and the influence of substrate effects at the thin edge of the cell.

Elastin Deficiency Reduces SMC Modulus. AFM was used to quantify the effect of elastin deficiency on SMC modulus in three separate trials. In each individual trial, the *Eln*-/- SMCs display a reduced modulus, up to 48%, compared to both *Eln*+/− and *Eln*+/+ SMCs. This reduction is significant for the *Eln*-/- SMCs in each trial when compared to the *Eln*+/+ genotype. The cumulative results of all trials are shown in Fig. 3. Overall, the average modulus of *Eln*-/- SMCs is significantly reduced 33% and 40% compared to *Eln*+/− and *Eln*+/+ values, respectively. No significant difference is observed between the modulus values of *Eln*+/− and *Eln*+/+ SMCs. These results indicate that the lack of expression of the elastin protein has a direct effect on the SMC modulus.

In contrast to the data for the elastin deficient SMCs, the trials with fibulin-4 deficient SMCs did not indicate any relationship

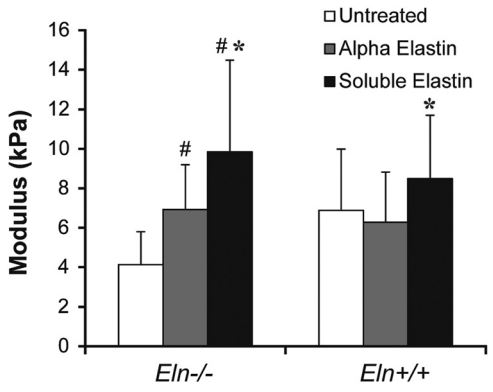

Fig. 5 Either elastin treatment increases the *Eln-/-* SMC modulus compared to untreated *Eln-/-* SMCs (# = $P < 0.05$). For both genotypes, soluble elastin treated SMCs have a higher modulus than those treated with α elastin (* = $P < 0.05$).

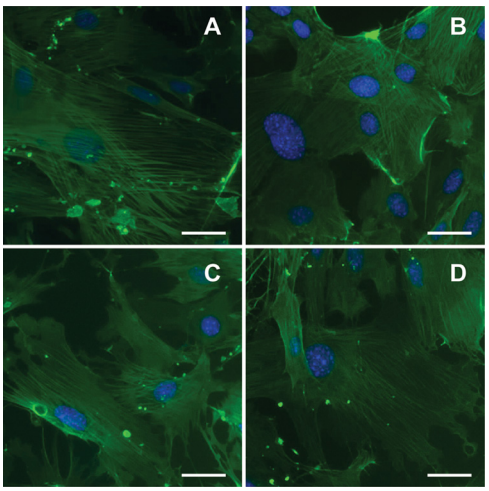

Fig. 6 Fluorescent staining does not reveal obvious differences in actin stress fiber density (green) between genotypes or treatments. Images are from untreated *Eln-/-* (*A*), untreated *Eln+/+* (*B*), α elastin treated *Eln-/-* (*C*), and α elastin *Eln+/+* (*D*) SMCs with the cell nuclei in blue. Scale bar = 50 μm.

between fibulin-4 deficiency and SMC modulus. Collective data from the three trials show similar modulus values across all fibulin-4 genotypes (Fig. 4).

Elastin Treatment Rescues the SMC Modulus. The addition of either soluble or α elastin increases the average Young's modulus of *Eln*-/- SMCs. The individual trials and overall data (Fig. 5) show that the Young's modulus of treated *Eln*-/- and *Eln*+/+ SMCs are comparable and that there is no significant difference between the genotypes. Compared to untreated *Eln*-/- SMCs, both α and soluble elastin treated *Eln*-/- SMCs have a significantly higher modulus. Additionally, soluble elastin treated SMCs for both genotypes have a significantly higher modulus than α elastin treated SMCs. Four trials were performed in the soluble elastin experiment due to the large standard deviation of the modulus for *Eln*-/- SMCs.

Elastin Genotype and Treatment Alters Gene Expression. Fluorescence microscopy did not show any obvious changes in the actin stress fiber density or organization between untreated and α elastin treated *Eln*-/- and *Eln*+/+ SMCs (Fig. 6). For more quantitative results, gene expression was analyzed using RT-PCR, which shows that expression of SMC contractile and synthetic genes differs between genotypes and treatment conditions (Fig. 7).

As expected, there is a 100% reduction in elastin expression for all treatment conditions for *Eln*-/- SMCs compared to untreated *Eln*+/+ SMCs (Fig. 7(*A*)). Additionally, soluble and α elastin treated *Eln*+/+ SMCs show a 90% and 82% reduction in *Eln* expression, respectively, compared to untreated *Eln*+/+ SMCs. *Col1a1* shows no significant differences across any of the groups and is therefore, not shown in Fig. 7. *Myocd*, known as a master regulator of SMC phenotype [23], is down regulated by 63% in untreated *Eln*-/- SMCs compared to untreated *Eln*+/+ SMCs, with no significant changes in either genotype due to elastin treatment. Several other genes, including *Fbln4*, *Myh10*, *Smtn*, and *Tagln*, also show significant expression differences between genotypes, but unlike *Myocd*, are affected by the elastin treatments (Fig. 7(*B*)). All of these genes have reduced expression in untreated *Eln*-/- SMCs compared to untreated *Eln*+/+ SMCs, and expression is down regulated in each genotype with elastin treatment. In addition, the expression of some genes is significantly different between elastin treatment types, especially for *Eln*-/- SMCs. These genes include *Aebp1*, *Cald1*, *Cdh2*, and *Myh11* (Fig. 7(*C*)). In some cases, α elastin treatment decreases expression in *Eln*-/- SMCs, while soluble elastin has little effect (i.e., *Aebp1*, *Cald1*, and *Cdh2*), compared to the untreated case. For *Myh11*, soluble elastin decreases expression in *Eln*-/- SMCs to 41% compared to the untreated case, while α elastin has little effect.

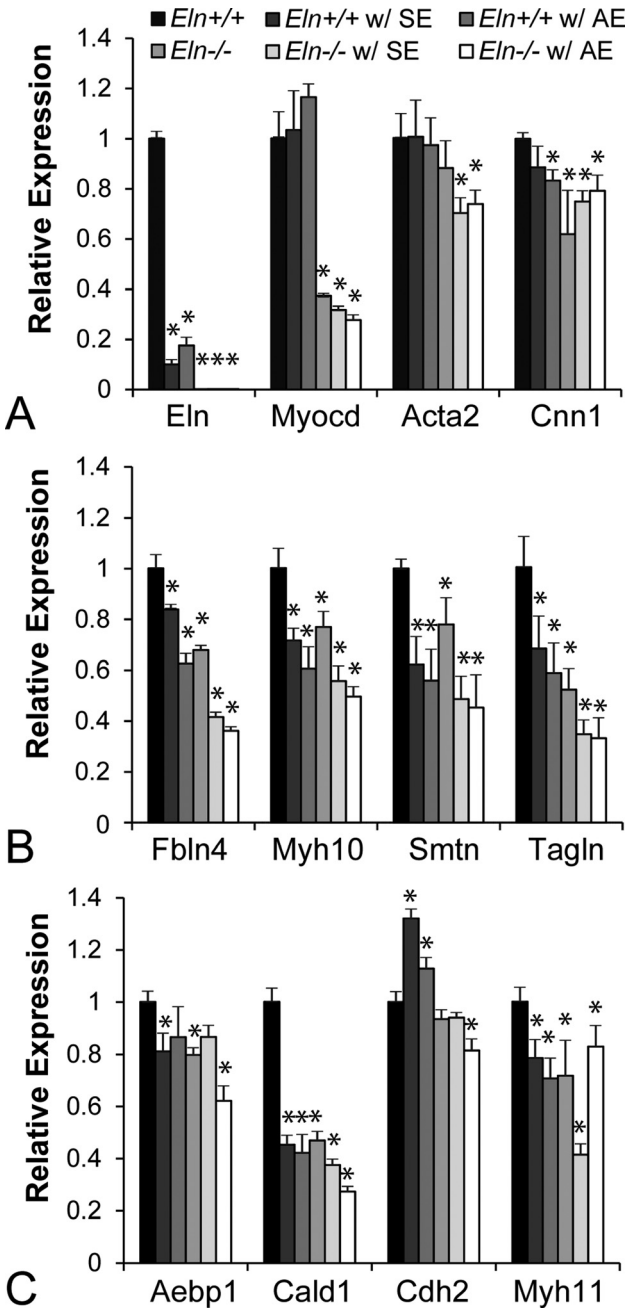

Fig. 7 Gene expression varies across genotype and treatment conditions. * = $P < 0.05$ compared to untreated *Eln*+/+ SMCs

Because elastin treatments increase the Young's modulus compared to the untreated case only in *Eln*-/- SMCs, perhaps the most interesting observations for the gene expression data can be made from instances where only the *Eln*-/- genotype is affected by treatment. Elastin treatment has no significant effect on *Acta2* or *Cnn1* expression in *Eln*+/+ SMCs (Fig. 7(*A*)). However, *Acta2* expression is significantly reduced and *Cnn1* expression is significantly increased for both elastin treatments in *Eln*-/- SMCs.

Discussion

Association Between Gene Expression and Modulus in *Eln*-/- SMCs. Mature SMCs with a contractile phenotype produce many of the proteins necessary for the formation of their

cytoskeleton [24]. SMCs may revert to a synthetic phenotype, which is characteristic of undifferentiated SMCs. SMCs with a synthetic phenotype tend to secrete ECM proteins instead of internal cytoskeletal proteins [25]. Therefore, it is feasible that phenotype modulation leads to changes in SMC modulus.

We posit that the loss of elastin production in *Eln*-/- SMCs causes them to shift toward a synthetic phenotype, which results in a reduced modulus. This is supported by previous work showing that *Eln*-/- SMCs have increased proliferation and less organized actin stress fibers [18]. Our data show that several genes, typically and highly expressed by mature SMCs, are significantly down regulated in *Eln*-/- SMCs. These contractile genes include *Cald1*, *Cdh2*, *Cnn1*, *Myh11*, *Myocd*, *Smtn*, and *Tagln*. Each of these genes is critical for the function and formation of the SMC cytoskeleton [1,23,26–28] and reduced expression may affect the cellular mechanical properties. Not all of the cytoskeletal genes are down regulated in *Eln*-/- SMCs. For example, expression of *Acta2,* the gene for SM α-actin, is similar in untreated *Eln*+/+ and *Eln*-/- SMCs. Unlike the work of Karnik et al. [18], fluorescence microscopy shows no indication that the amount of actin stress fibers varies with genotype. However, actin stress fibers can be highly variable between individual SMCs and many of the genes interact during formation of the cytoskeleton, so no one single gene can determine SMC phenotype. In this case, *Tagln*, the gene for SM 22, is down regulated in *Eln*-/- SMCs which can result in thinner and more dispersed actin stress fibers [26], and may alter the cellular mechanical properties without reducing the number of stress fibers or causing changes that are visible by fluorescence microscopy.

Effects of Exogenous Elastin Treatments. SMCs respond to the 20–25 h incubation of 0.16 mg/ml soluble or α elastin cell culture media with changes in gene expression. Karnik et al. [18] showed a dose dependent response of *Eln*-/- SMC proliferation to soluble elastin concentrations with a maximum at 0.10 mg/ml, near our chosen concentration, with significant effects by 24 h. Additionally, tumor cell lines have been shown to decrease and delay their adhesion to a 0.2 mg/ml soluble elastin coated surface after a 24 h incubation period [19]. Experiments with other incubation times or concentrations were not performed in the current study, but would be interesting to explore in the future. At the specified experimental conditions, elastin expression in treated *Eln*+/+ SMCs is significantly reduced. This implies that SMCs are able to sense the presence of elastin in the environment and determine when additional elastin production is necessary. This may be done by triggering a signaling cascade. Previous research has suggested potential pathways, such as those involving Rho or ERK1/2 activation [18,29]. *Eln*+/+ SMC expression of *Fbln4*, a gene necessary for proper assembly of the elastic fibers [5], is also significantly down regulated in the presence of elastin. It is possible that the detection of elastin in the environment signals that there is no further need for elastic fiber formation.

It is important to note that elastin treatment causes the reduction in expression of several synthetic genes in *Eln*-/- SMCs. For example, *Myh10* is down regulated in response to both elastin treatments, while *Aebp1* expression is reduced only due to α elastin treatment. Down regulation of these synthetic genes suggests that the treatments may cause a shift towards a contractile phenotype and may partially explain the increase in modulus for treated *Eln*-/- SMCs in the AFM experiments. Previous work also showed that treatment with soluble or α elastin encourages a contractile phenotype in *Eln*-/- SMCs by decreasing proliferation and increasing actin stress fibers [18]. Although the treatment based changes in Young's modulus occurred only in *Eln*-/- SMCs, SMCs from both genotypes altered their gene expression in response to exogenous elastin. This suggests that the particular set of gene changes measured in the current work does not affect the modulus in healthy *Eln*+/+ SMCs. However, the combination of elastin deficiency and gene expression changes may contribute to a still unknown pathway that is linked to SMC modulus.

***Cnn1* and *Myh11* Correlation With SMC Modulus.** The addition of insoluble α elastin or soluble tropoelastin to the cell culture media reverses the effects of elastin insufficiency and increase the Young's modulus in *Eln*-/- SMCs by 65% and 120%, respectively. *Cnn1* expression best correlates with the measured mechanical properties of *Eln*-/- and *Eln*+/+ SMCs before and after the elastin treatments. *Cnn1* expression shows little to no changes in treated *Eln*+/+ SMCs, but is significantly increased after treatment in *Eln*-/- SMCs. *Cnn1* codes for calponin, which is colocalized with actin stress fibers and is known to regulate SMC contractility via inhibition of actomyosin ATPase [30]. Additionally, calponin has been found to interact with mitogen-activated protein kinase (MAPK) [31], thus showing a link between *Cnn1* and *Eln* through the ERK1/2 pathway. This may be part of the genetic mechanism that relates elastin deficiency to both SMC phenotype and modulus.

The significant difference in modulus between the two elastin treatments in *Eln*-/- SMCs may be explained by the difference in expression of *Aebp1*, *Cald1*, *Cdh2*, and *Myh11*. In the case of *Myh11*, expression jumps from 41% of untreated *Eln*+/+ values for soluble elastin to 83% for α elastin treated *Eln*-/- SMCs. Both *Eln* and *Myh11* expression have previously been linked to the Rho signaling pathway [27]. Therefore, the SMC modulus and gene expression changes in response to the elastin treatments may be associated with Rho mediated myosin heavy chain synthesis, activated by an elastin receptor capable of detecting the difference between soluble and crosslinked elastin. These data may begin to elucidate the role or importance of elastin crosslinking in the modulation of SMC phenotype and modulus.

Study Limitations and Connections to Human Disease. AFM data were analyzed using the Hertz model of contact between a sphere and a flat surface. Although the Hertz model is the most popular approach to force curve analysis, its assumptions are quite stringent. The indented sample is assumed to be isotropic and linearly elastic, characteristics that are generally not found in biological samples, such as cells [32]. Its use is justified by the experimental design. At small deformations, the assumption of linear and isotropic behavior has increased validity. Therefore, a spherical indenter was used as opposed to a pyramidal or conical tip, which causes greater deformation and possibly even membrane rupture. Additionally, the use of a spherical indenter not only ensures shallow indentations, but also a significantly larger contact area. This begins to alleviate concerns about the localized nature of AFM studies. The 5 μm diameter bead was selected because of its large contact area, but low weight on the cantilever.

Mouse models provide convenient methods for investigating the effects of single gene deficiencies, but they are not completely representative of human diseases that may be caused by a combination of genetic, epigenetic, environmental, chemical, and other causes. Isolated SMCs are not in their native three-dimensional arterial wall environment and this may influence SMC modulus and gene expression. In fact, previous work quantifying gene expression in *Eln*-/- aorta found increases in expression of *Acta2*, *Myh11*, and *Myocd* compared to *Eln*+/+aorta [11], while we found decreases in these genes for isolated *Eln*-/- SMCs compared to *Eln*+/+ SMCs. Nonetheless, the work presented here provides a starting point for investigating links between elastin deficiency, SMC gene expression, SMC modulus, and large artery stiffness.

Initially, it is unclear how a decrease in SMC modulus may lead to an increase in arterial stiffness. Although individual *Eln*-/- SMCs have a reduced modulus, they will most likely proliferate at a greater rate, which is typical of SMCs with a synthetic phenotype. Therefore, hyperplasia of dedifferentiated SMCs may lead to an increase in arterial muscle mass and stiffness. Although the current work is most applicable to the understanding and treatment of diseases involving elastin deficiency, such as supravalvular aortic stenosis, the data can be broadly applied to hypertension

research because of the connection between high blood pressure and increased arterial stiffness [1]. The current data could be used to investigate treatment strategies that would decrease arterial wall stiffness by maintaining SMCs in a contractile phenotype.

Conclusion

Elastin deficiency, and not fibulin-4 deficiency, results in a reduced Young's modulus in isolated arterial SMCs, as measured by AFM. The modulus is rescued in *Eln*-/- SMCs by treatment with exogenous soluble or α elastin, indicating that SMCs can sense and respond mechanically to elastin in various forms in the environment. Gene expression results provide insight into genetic mechanisms underlying the reduced modulus in *Eln*-/- SMCs and the rescued modulus with elastin treatments. Decreased expression of calponin (*Cnn1*) in untreated *Eln*-/- SMCs, along with increased *Cnn1* expression after elastin treatment provides the most direct link for a genetic mechanism that mediates cell modulus. The data are important for understanding relationships between SMC modulus and gene expression, and how SMC properties may impact mechanical behavior of the arterial wall.

Acknowledgment

Dr. Robert Mecham at Washington University and Dr. Dean Li at the University of Utah kindly provided the *Eln*+/− mice. We thank Dr. Gerald Meininger at the University of Missouri for assistance in setting up the AFM experiments. The AFM was acquired through NSF MRI No. 0619184 to Dr. Rebecca Willits. This work was supported by NIH R01HL115560 (J.E.W.), R01HL105314 (J.E.W.), and R01HL106305 (H.Y.).

References

[1] Wagenseil, J. E., and Mecham, R. P., 2009, "Vascular Extracellular Matrix and Arterial Mechanics," Physiol. Rev., **89**(3), pp. 957–989.
[2] Glagov, S., Vito, R., Giddens, D. P., and Zarins, C. K., 1992, "Micro-Architecture and Composition of Artery Walls: Relationship to Location, Diameter and the Distribution of Mechanical Stress," J. Hypertens. Suppl., **10**(6), pp. S101–S104.
[3] Standley, P. R., Camaratta, A., Nolan, B. P., Purgason, C. T., and Stanley, M. A., 2002, "Cyclic Stretch Induces Vascular Smooth Muscle Cell Alignment via No Signaling," Am. J. Physiol., Heart and Circulatory Physiol., **283**(5), pp. H1907–H1914.
[4] Wolinsky, H., and Glagov, S., 1967, "A Lamellar Unit of Aortic Medial Structure and Function in Mammals," Circ. Res., **20**(1), pp. 99–111.
[5] Wagenseil, J. E., and Mecham, R. P., 2007, "New Insights into Elastic Fiber Assembly," Birth Defects Res. C Embryo Today, **81**(4), pp. 229–240.
[6] Li, D. Y., Brooke, B., Davis, E. C., Mecham, R. P., Sorensen, L. K., Boak, B. B., Eichwald, E., and Keating, M. T., 1998, "Elastin is an Essential Determinant of Arterial Morphogenesis," Nature, **393**(6682), pp. 276–280.
[7] Wagenseil, J. E., Nerurkar, N. L., Knutsen, R. H., Okamoto, R. J., Li, D. Y., and Mecham, R. P., 2005, "Effects of Elastin Haploinsufficiency on the Mechanical Behavior of Mouse Arteries," Am. J. Physiol. Heart Circ. Physiol., **289**(3), pp. H1209–H1217.
[8] Li, D. Y., Faury, G., Taylor, D. G., Davis, E. C., Boyle, W. A., Mecham, R. P., Stenzel, P., Boak, B., and Keating, M. T., 1998, "Novel Arterial Pathology in Mice and Humans Hemizygous for Elastin," J. Clin. Invest., **102**(10), pp. 1783–1787.
[9] Li, D. Y., Toland, A. E., Boak, B. B., Atkinson, D. L., Ensing, G. J., Morris, C. A., and Keating, M. T., 1997, "Elastin Point Mutations Cause an Obstructive Vascular Disease, Supravalvular Aortic Stenosis," Human Mol. Genet., **6**(7), pp. 1021–1028.
[10] Mclaughlin, P. J., Chen, Q., Horiguchi, M., Starcher, B. C., Stanton, J. B., Broekelmann, T. J., Marmorstein, A. D., McKay, B., Mecham, R., Nakamura, T., and Marmorstein, L. Y., 2006, "Targeted Disruption of Fibulin-4 Abolishes Elastogenesis and Causes Perinatal Lethality in Mice," Mol. Cell Biol., **26**(5), pp. 1700–1709.
[11] Huang, J., Davis, E. C., Chapman, S. L., Budatha, M., Marmorstein, L. Y., Word, R. A., and Yanagisawa, H., 2010, "Fibulin-4 Deficiency Results in Ascending Aortic Aneurysms: A Potential Link between Abnormal Smooth Muscle Cell Phenotype and Aneurysm Progression," Circ. Res., **106**(3), pp. 583–592.
[12] Hucthagowder, V., Sausgruber, N., Kim, K. H., Angle, B., Marmorstein, L. Y., and Urban, Z., 2006, "Fibulin-4: A Novel Gene for an Autosomal Recessive Cutis Laxa Syndrome," Am. J. Human Genet., **78**(6), pp. 1075–1080.
[13] Wagenseil, J. E., Ciliberto, C. H., Knutsen, R. H., Levy, M. A., Kovacs, A., and Mecham, R. P., 2009, "Reduced Vessel Elasticity Alters Cardiovascular Structure and Function in Newborn Mice," Circ. Res., **104**(10), pp. 1217–1224.
[14] Huang, J., Yamashiro, Y., Papke, C. L., Ikeda, Y., Lin, Y., Patel, M., Inagami, T., Le, V. P., Wagenseil, J. E., and Yanagisawa, H., 2013, "Angiotensin-Converting Enzyme-Induced Activation of Local Angiotensin Signaling is Required for Ascending Aortic Aneurysms in Fibulin-4-Deficient Mice," Sci. Transl. Med., **5**(183), p. 018358.
[15] Martens, J. C., and Radmacher, M., 2008, "Softening of the Actin Cytoskeleton by Inhibition of Myosin Ii," Pflugers Arch., **456**(1), pp. 95–100.
[16] Prabhune, M., Belge, G., Dotzauer, A., Bullerdiek, J., and Radmacher, M., 2012, "Comparison of Mechanical Properties of Normal and Malignant Thyroid Cells," Micron, **43**(12), pp. 1267–1272.
[17] Qiu, H., Zhu, Y., Sun, Z., Trzeciakowski, J. P., Gansner, M., Depre, C., Resuello, R. R., Natividad, F. F., Hunter, W. C., Genin, G. M., Elson, E. L., Vatner, D. E., Meininger, G. A., and Vatner, S. F., 2010, "Short Communication: Vascular Smooth Muscle Cell Stiffness as a Mechanism for Increased Aortic Stiffness With Aging," Circ. Res., **107**(5), pp. 615–619.
[18] Karnik, S. K., Brooke, B. S., Bayes-Genis, A., Sorensen, L., Wythe, J. D., Schwartz, R. S., Keating, M. T., and Li, D. Y., 2003, "A Critical Role for Elastin Signaling in Vascular Morphogenesis and Disease," Development, **130**(2), pp. 411–423.
[19] Svitkina, T. M., and Parsons, D. F., 1993, "Binding of Some Metastatic Tumor Cell Lines to Fibrous Elastin and Elastin Peptides," Int. J. Cancer, **53**(5), pp. 824–828.
[20] Sun, Z., Martinez-Lemus, L. A., Trache, A., Trzeciakowski, J. P., Davis, G. E., Pohl, U., and Meininger, G. A., 2005, "Mechanical Properties of the Interaction between Fibronectin and $\alpha_5\beta_1$-Integrin on Vascular Smooth Muscle Cells Studied Using Atomic Force Microscopy," Am. J. Physiol. Heart Circ. Physiol., **289**(6), pp. H2526–H2535.
[21] Sader, J. E., 1995, "Parallel Beam Approximation for V-Shaped Atomic-Force Microscope Cantilevers," Rev. Sci. Instrum., **66**(9), pp. 4583–4587.
[22] Costa, K. D., 2006, "Imaging and Probing Cell Mechanical Properties With the Atomic Force Microscope," Methods Mol. Biol., **319**, pp. 331–361.
[23] Wang, Z., Wang, D. Z., Pipes, G. C., and Olson, E. N., 2003, "Myocardin Is a Master Regulator of Smooth Muscle Gene Expression," Proc. Natl. Acad. Sci. USA, **100**(12), pp. 7129–7134.
[24] Wright, D. B., Trian, T., Siddiqui, S., Pascoe, C. D., Johnson, J. R., Dekkers, B. G., Dakshinamurti, S., Bagchi, R., Burgess, J. K., Kanabar, V., and Ojo, O. O., 2013, "Phenotype Modulation of Airway Smooth Muscle in Asthma," Pulmonary Pharmacol. Therapeutics, **26**(1), pp. 42–49.
[25] Stegemann, J. P., Hong, H., and Nerem, R. M., 2005, "Mechanical, Biochemical, and Extracellular Matrix Effects on Vascular Smooth Muscle Cell Phenotype," J. Appl. Physiol., **98**(6), pp. 2321–2327.
[26] Han, M., Dong, L. H., Zheng, B., Shi, J. H., Wen, J. K., and Cheng, Y., 2009, "Smooth Muscle 22 Alpha Maintains the Differentiated Phenotype of Vascular Smooth Muscle Cells by Inducing Filamentous Actin Bundling," Life Sci., **84**(13–14), pp. 394–401.
[27] Kuang, S. Q., Kwartler, C. S., Byanova, K. L., Pham, J., Gong, L., Prakash, S. K., Huang, J., Kamm, K. E., Stull, J. T., Sweeney, H. L., and Milewicz, D. M., 2012, "Rare, Nonsynonymous Variant in the Smooth Muscle-Specific Isoform of Myosin Heavy Chain, Myh11, R247c, Alters Force Generation in the Aorta and Phenotype of Smooth Muscle Cells," Circ. Res., **110**(11), pp. 1411–1422.
[28] Mayanagi, T., and Sobue, K., 2011, "Diversification of Caldesmon-Linked Actin Cytoskeleton in Cell Motility," Cell Adh. Migr., **5**(2), pp. 150–159.
[29] Lin, S., and Mequanint, K., 2012, "The Role of Ras-Erk-Il-1beta Signaling Pathway in Upregulation of Elastin Expression by Human Coronary Artery Smooth Muscle Cells Cultured in 3d Scaffolds," Biomaterials, **33**(29), pp. 7047–7056.
[30] Gimona, M., Herzog, M., Vandekerckhove, J., and Small, J. V., 1990, "Smooth Muscle Specific Expression of Calponin," FEBS Lett., **274**(1–2), pp. 159–162.
[31] Menice, C. B., Hulvershorn, J., Adam, L. P., Wang, C. A., and Morgan, K. G., 1997, "Calponin and Mitogen-Activated Protein Kinase Signaling in Differentiated Vascular Smooth Muscle," J. Biol. Chem., **272**(40), pp. 25157–12561.
[32] Azeloglu, E. U., and Costa, K. D., 2011, "Atomic Force Microscopy in Mechanobiology: Measuring Microelastic Heterogeneity of Living Cells," Methods Mol. Biol., **736**, pp. 303–329.